

Integrated Nonlinear Hierarchical Control and Management of Hybrid AC/DC Microgrids

Biglarahmadi, Mojtaba; Ketabi, Abbas; Reza Baghaee, Hamid; Guerrero, Josep M.

Published in:
IEEE Systems Journal

DOI (link to publication from Publisher):
[10.1109/JSYST.2021.3050334](https://doi.org/10.1109/JSYST.2021.3050334)

Publication date:
2022

Document Version
Accepted author manuscript, peer reviewed version

[Link to publication from Aalborg University](#)

Citation for published version (APA):

Biglarahmadi, M., Ketabi, A., Reza Baghaee, H., & Guerrero, J. M. (2022). Integrated Nonlinear Hierarchical Control and Management of Hybrid AC/DC Microgrids. *IEEE Systems Journal*, 16(1), 902-913. <https://doi.org/10.1109/JSYST.2021.3050334>

General rights




Copyright and moral rights for the publications made accessible in the public portal are retained by the authors and/or other copyright owners and it is a condition of accessing publications that users recognise and abide by the legal requirements associated with these rights.

- Users may download and print one copy of any publication from the public portal for the purpose of private study or research.
- You may not further distribute the material or use it for any profit-making activity or commercial gain
- You may freely distribute the URL identifying the publication in the public portal -

Take down policy

If you believe that this document breaches copyright please contact us at vbn@aub.aau.dk providing details, and we will remove access to the work immediately and investigate your claim.

Integrated Nonlinear Hierarchical Control and Management of Hybrid AC/DC Microgrids

Mojtaba Biglarahmadi, Abbas Ketabi , *Member, IEEE*, Hamid Reza Baghaee , *Member, IEEE*,
and Josep M. Guerrero , *Fellow, IEEE*

Abstract—Increasing the usage of distributed generations (DGs) leads the microgrids (MGs) to develop. Considering the existence of alternating current (ac) loads and sources and concerning increasing direct current (dc) loads and sources, hybrid ac/dc MGs have been used to have the advantages of both ac and dc MGs and reduce the drawbacks of them. By integrating the DG units in hybrid ac/dc MGs. Hence, a proper control method is required in such MGs to achieve precise voltage regulation and power-sharing, desired power quality, high efficiency, and high reliability. This article focused on nonlinear exponential control and distributed secondary control schemes to properly control the MG and form an integrated nonlinear hierarchical control and management for hybrid ac/dc MGs. Finally, to evaluate the proposed nonlinear control strategy's performance, offline digital time-domain simulation studies are carried out on a test MG system in MATLAB/Simulink environment. The results are also compared with previously reported methods. The simulation results and the comparisons showed that the proposed methods could properly share the power among subgrids and DGs in both ac and dc subgrids. In contrast, the proposed control scheme can prove its effectiveness and superiority over conventional controllers.

Index Terms—Distributed control, frequency regulation, hybrid ac/dc microgrid (MG), nonlinear control, power-sharing, voltage regulation.

$\Delta f_s^*, V_s^*$
 P_{0x}, Q_{0x}

v_o, i_o, i_L

R_f, L_f, C_f

$\Delta v_{\max}, i_{\max}$

P_{dc}, P_{dc}^*
 $v_{cb}^*, v_{cb}^{\max}, v_{cb}^{\min}$

NOMENCLATURE

Rated frequency and voltage deviations.
Rated active power and rated reactive power.
Output voltage, output current, and filter current.
Filter resistance, inductance and capacitance.
Maximum voltage derivation and output current.
output power, and nominal output power.
Nominal, maximum and minimum voltage of common bus.

f^*, f^{\max}, f^{\min}

$v_{dc}^*, v_{dc}^{\max}, v_{dc}^{\min}$

m_P, n_Q, m_P, n_Q, r
 $e_{vi}, e_{\omega i}, e_{vi}^V, e_{vi}^u, e_{Pi}$

g_i

ω_c

$u_{vi}, u_{\omega i}$

c_P, c_v, c_ω

V^*, i_i

N_t

α_i, β_i

$v^{\text{ref}}, f^{\text{ref}}$

δf

$v_{dc}^{\text{ref}}, v_{dc}^*, i_{dc}$

Nominal, the maximum and minimum frequency.

Nominal, maximum and minimum dc voltage.

Droop coefficients.

Local neighborhood tracking, control input consensus and local neighborhood tracking error

Pinning gain,

Cut-off frequency of low-pass filters.

Auxiliary control signals.

Active power, voltage/frequency control gain.

Nominal dc voltage and dc output current.

Number of neighbors of i th DG.

Mixed error coefficients.

Reference voltage and frequency.

Coordinated control signal.

Reference and nominal dc output voltage, measured output dc current.

I. INTRODUCTION

THE hybrid microgrid (MG) can exploit the prominent features of both ac and dc MGs. In a hybrid, ac/dc MG, the power-sharing among distributed generation (DG) units and precise power-sharing among ac and dc subgrids is required. Among all strategies reported for ac and dc MGs, nonlinear control, and distributed secondary control schemes attracted researchers' attention [1].

In ac MGs, nonlinear and adaptive droop control strategies have been used in the secondary [2] and primary control level [3]–[7], for control of wind power generation unit to participate in MG frequency control [3], primary voltage/frequency stabilization [4], [6], enhancing active/reactive power-sharing [5], [8], harmonic power-sharing [9], [10], and optimizing MG operation [7]. Nonlinear and adaptive droop control techniques have also been investigated for dc MGs for decentralized control [11], distributed control [12], decentralized load sharing [13], and voltage control and load sharing [14]. Another nonlinear control strategy based on sliding mode control (SMC) has also been reported in [15].

Nonlinear control strategies have been used for the control of interlinking converters (ICs), and hybrid MGs [16]–[19]. In [20], a new control scheme has been introduced based on a robust nonlinear state feedback control concept for robust control of a bidirectional interlinking converter (BICs) in a hybrid ac/dc MGs. In this regard, an adaptive power-sharing mechanism had been presented for maintaining the low voltage

Manuscript received July 13, 2020; revised October 25, 2020 and December 28, 2020; accepted January 5, 2021. This work was supported by VILLUM FONDEN under the VILLUM Investigator under Grant 25920, Center for Research on Microgrids. (Corresponding author: Abbas Ketabi.)

Mojtaba Biglarahmadi and Abbas Ketabi are with the Department of Electrical Engineering, University of Kashan, Kashan 8731753153, Iran (e-mail: mojtaba.biglarahmadi66@gmail.com; aketabi@kashanu.ac.ir).

Hamid Reza Baghaee is with the Department of Electrical Engineering, Amirkabir University of Technology, Tehran 15875-4413, Iran (e-mail: hrbaghaee@aut.ac.ir).

Josep M. Guerrero is with the Department of Energy Technology, Aalborg University, Aalborg 9220, Denmark (e-mail: joz@et.aau.dk).

Digital Object Identifier 10.1109/JSYST.2021.3050334

dc (LVdc) voltage under control, not only reducing the stress in the central battery system and its dependence on the utility grid but also demonstrating the extended operation and improved transient response in the LVdc when the central battery systems present bandwidth and power limitations. Robust power management and nonlinear SMC strategies have been proposed in [1] and [16], to improve small- and large-signal stability, enhance power-sharing, and improve the performance of ac and hybrid ac/dc MGs, respectively, for nonlinear and unbalanced loads. In [16], besides sliding mode controller for dc/dc converters, two separate controllers have been designed for positive sequence power control and negative sequence current control based on the SMC and Lyapunov function theory, respectively, for the sake of enhancing power-sharing and regulating active and reactive powers injected by distributed energy resources, and controlling harmonic and negative-sequence current in the presence of nonlinear and unbalanced voltage control has also been introduced in [21] for a hybrid ac/dc MG, which does not need the remote measurement or communication with a plug-and-play functionality.

The secondary control level will restore the primary layer's fluctuations to regulate islanded MG voltage and frequency [17]–[19]. Distributed control has been widely discussed in the literature for the secondary restoration of voltage and frequency [2], [22], active power-sharing [23], reactive power-sharing [24], and balancing the state of charge (SoC) of the energy storage system (ESS) [25]–[29]. Recently, different aspects of distributed secondary control of MG, such as time-delay [25], [30], noise-resiliency [28], [31], fault-tolerant control [27], [32], and finite-time consensus [2], [33], have been addressed in the literature. In [34], a nonlinear hierarchical scheme has been presented for an unreliable communication network for jointly-connected switching topologies, which can greatly improve the system's reliability. A robust strategy such as the SMC strategy has been used in the secondary layer for disturbance rejection and controlling the SoC of battery ESSs (BESS) considering parametric uncertainties of MG [35]. Also, different kinds of the literature have studied distributed secondary control of dc MGs [28]–[30] for achieving proportional power-sharing and improve the voltage regulation [36], accurate power allocation [37], and managing the SoC of ESSs [38], [39].

Different distributed secondary control schemes and nonlinear control techniques have been proposed for ac or dc MGs. However, few pieces of research have considered these control techniques in a hybrid ac/dc MG with focusing on power-sharing among ac and dc subgrids [40], distributed control and power management [40], [41], and intelligent multiagent system (MAS) based control [42].

In the previous literature, the issues concerning power quality, voltage and frequency regulation of ac DGs, precise power-sharing in ac subgrid, voltage regulation of dc DGs, and load sharing in the dc subgrid have not been considered simultaneously. The main contribution of this article is to present a nonlinear-based primary control scheme for a test MG system to regulate the dc and ac voltages and ac frequency of MG, improve the power quality, and enhance the load sharing. This control method is compared with conventional droop based primary controllers. Then, a distributed secondary control is applied to them for more precise comparison. When the nonlinear method is exploited for ac and dc DGs, the BICs are also controlled in a nonlinear manner. The proposed integrated nonlinear hierarchical control scheme is simulated in MATLAB/Simulink software

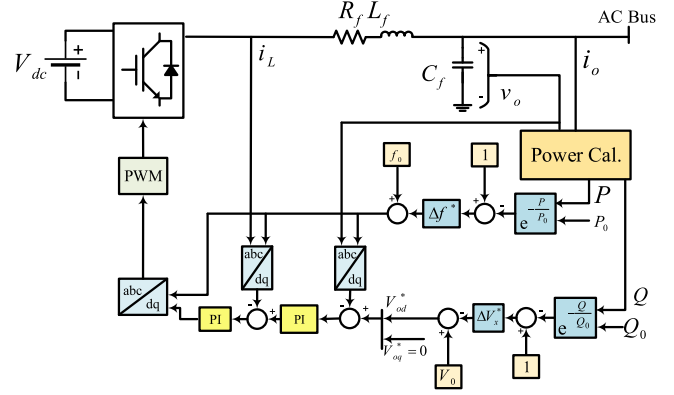


Fig. 1. Control of ac DG based on the proposed nonlinear exponential strategy.

environment for a test MG (including ac subgrid with multiple ac DGs, dc subgrid with multiple dc DGs, bidirectional ac/dc, and dc/dc converters, which connect the ac and dc subgrids, and a storage system). Also, its performance is compared with conventional control strategies.

II. PROPOSED NONLINEAR PRIMARY CONTROL

A. Nonlinear Controlled DGs in AC Subgrid

The conventional droop control method can provide active/reactive power-sharing among inverter-based DGs. Still, applying it has some limitations and has some deviations in reactive power-sharing [6]. On the other hand, the high R/X ratio of distribution lines affects the droop control not to work correctly. So, in this section, to overcome the inherent drawbacks of the conventional droop control method, improve MG stability margins, and overcome the effects of line impedances on reactive power-sharing, an exponential-based droop control strategy is proposed for DG units in the ac subgrid as follows (see Fig. 1):

$$f_x = f_0 - \Delta f_x^* \left(1 - e^{-\frac{P_x}{k P_{0x}}}\right)$$

$$V_x = V_0 - \Delta V_x^* \left(1 - e^{-\frac{Q_x}{k Q_{0x}}}\right) \quad (1)$$

$$\Delta f_x^* = C_1 \frac{\Delta V_x^*}{k Q_{0x}} = C_2 \quad (2)$$

where k , C_1 , and C_2 are the constant values. Differentiating (1), yields

$$\dot{V}_x = -\frac{\Delta V_x^*}{k Q_{0x}} e^{-\frac{Q_x}{k Q_{0x}}} \quad (3)$$

All DGs should operate in a similar voltage change in the steady-state. Thus, we have

$$\dot{V}_1 = \dot{V}_2 \Rightarrow -\frac{\Delta V_1^*}{k Q_{01}} e^{-\frac{Q_1}{k Q_{01}}} = -\frac{\Delta V_2^*}{k Q_{02}} e^{-\frac{Q_2}{k Q_{02}}} \quad (4)$$

The following equation should be satisfied to meet precise reactive power-sharing among DGs:

$$-C e^{-\frac{Q_1}{k Q_{01}}} = -C e^{-\frac{Q_2}{k Q_{02}}} \Rightarrow \frac{Q_1}{Q_{01}} = \frac{Q_2}{Q_{02}} \quad (5)$$

where $C = \Delta V_1^*/(k Q_{01}) = \Delta V_2^*/(k Q_{02})$. As observed, the reactive output power of DG is associated with their rated

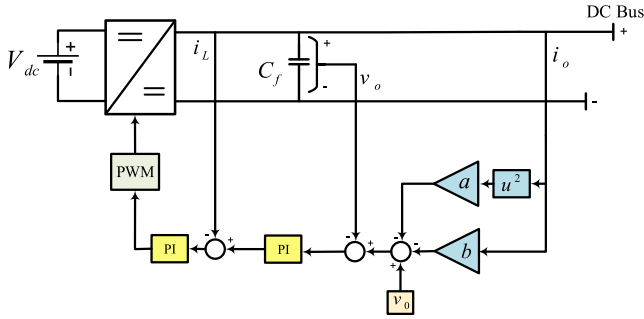


Fig. 2. Control of dc DG based on nonlinear strategy.

reactive power capacities. Moreover, the frequency of DGs is also identical in the steady-state too, and we have

$$f_1 = f_2 \Rightarrow$$

$$f_0 - \Delta f_1^* \left(1 - e^{-\frac{P_1}{k P_{01}}}\right) = f_0 - \Delta f_2^* \left(1 - e^{-\frac{P_2}{k P_{02}}}\right). \quad (6)$$

The active output power of DGs should satisfy

$$\frac{P_1}{P_{01}} = \frac{P_2}{P_{02}}. \quad (7)$$

So, the active output power of DGs is associated with their rated active power capacities, too. Based on the above equations, the frequency and voltage regulation and accurate power-sharing can be achieved if their associated variations are located in their prescribed limitations.

B. Nonlinear Control DGs in DC Subgrid

In this part of the analysis, a nonlinear droop curve is proposed to control the dc subgrid DGs. In this article, motivated by [14] and [43], a piecewise quadratic polynomial droop curves method is proposed to provide current sharing between DGs in dc subgrid, based on

$$v = v_0 - a i^2 - b i \quad (8)$$

where a and b are the cure coefficients. All DGs should have identical voltage in steady-state operation. Therefore

$$v_1 = v_2 \Rightarrow a_1 i_1^2 + b_1 i_1 = a_2 i_2^2 + b_2 i_2. \quad (9)$$

To guarantee accurate current sharing, we should have

$$\frac{i_1}{i_2} = \frac{P_1}{P_2}. \quad (10)$$

Also, we propose the following elliptic type of voltage compensation criteria:

$$\Delta V = \Delta v_{\max} - \Delta v_{\max} \sqrt{1 - \left(\frac{i}{i_{\max}}\right)^2}. \quad (11)$$

Employing the quadratic characteristic improves current sharing accuracy, and voltage compensation can be achieved (see Fig. 2).

C. Control of ESSs

The ESS (here, BESS) is employed to maintain the common bus's voltage and balance the power among ac and dc subgrids. A BESS is connected to the common bus through a bidirectional dc/dc converter. In this article, dissimilar to other reported papers, improved droop control is proposed to control the voltage

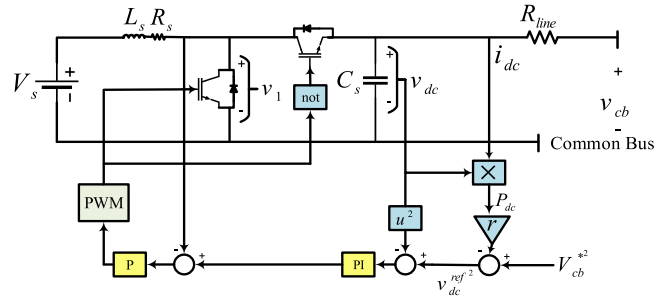


Fig. 3. Control of storage system based on improved droop strategy.

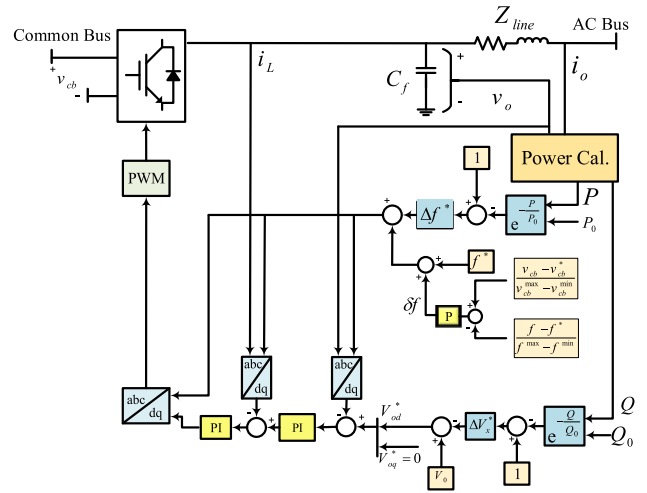


Fig. 4. Control of ac/dc BIC based on the proposed nonlinear exponential strategy.

as follows [44] (see Fig. 3):

$$v_{dc}^{ref2} = V_{cb}^{*2} - r(P_{dc} - P_{dc}^*). \quad (12)$$

As shown in Fig. 3, the control scheme has two inner and outer loops that the outer one obtains the reference value for the inner loop. The nominal power is considered zero here.

D. Control of AC/DC Bidirectional Interlink Converter

The ac/dc BIC maintains the voltage support for the ac subgrid. In this article, a nonlinear control is exploited similarly to ac DGs, which has a correction term added to the frequency term, named as coordinated control as [44]

$$f = (f_0 + \delta f) - \Delta f^* \left(1 - e^{-\frac{P_0 - P_x}{P_0}}\right) \quad (13)$$

$$V = V_0 - \Delta V^* \left(1 - e^{-\frac{Q_0 - Q_x}{Q_0}}\right)$$

where δf is obtained from coordinated control, and used for appropriate power-sharing among ac and dc subgrids and is expressed as

$$\delta f = \left(k_p + \frac{k_i}{s}\right) \left(\frac{v_{cb} - v_{cb}^*}{v_{cb}^{\max} - v_{cb}^{\min}} - \frac{f - f^*}{f^{\max} - f^{\min}}\right). \quad (14)$$

The control scheme of the ac/dc BIC is illustrated in Fig. 4.

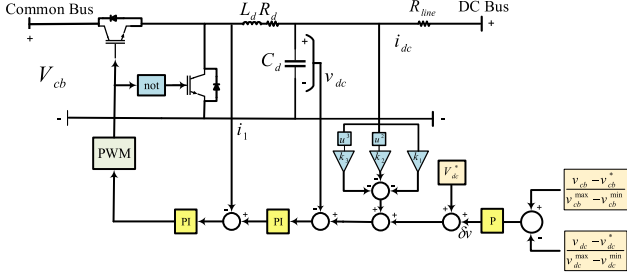


Fig. 5. Control of dc/dc BIC based on the proposed nonlinear strategy.

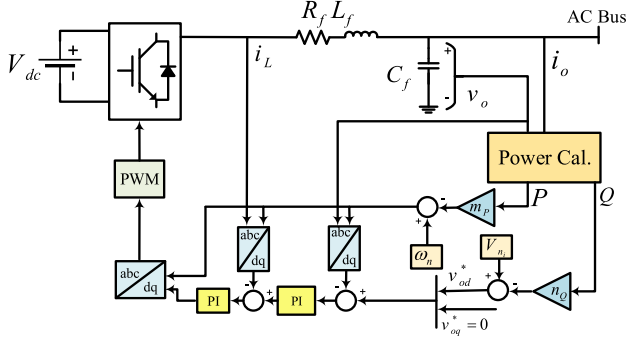


Fig. 6. Control of DG in ac subgrid with primary droop control.

E. Control of Bidirectional DC/DC Converter

The control structure of dc/dc BIC is illustrated in Fig. 5. The converter's low voltage side is connected to the dc bus, and the other side is connected to the common bus. The proposed nonlinear droop control is expressed as follows:

$$v = (V_0 + \delta v) - \sum_{n=1}^N k_n \cdot i^n \quad (15)$$

where k_n is parameters of nonlinear droop and $N = 3$. δv is the result of coordinated control and is defined as follows:

$$\delta v = \left(k_p + \frac{k_i}{s} \right) \left(\frac{v_{cb} - v_{cb}^*}{v_{cb}^{\max} - v_{cb}^{\min}} - \frac{v_{dc} - v_{dc}^*}{v_{dc}^{\max} - v_{dc}^{\min}} \right). \quad (16)$$

III. DISTRIBUTED SECONDARY CONTROL

A. Secondary Control of DGs in AC Subgrid

The hierarchical structure of DGs in the ac subgrid of hybrid ac/dc MG has two layers. The first layer shares the powers among DGs, and the second one restores the voltage and frequency fluctuations caused by the primary controller. The conventional droop method described by (17) is employed for primary control (see Fig. 6) [27], [31]

$$v = V_n - n_Q Q \quad \omega = \omega_n - m_P P. \quad (17)$$

The communication network is modeled by a graph that DGs are considered as its nodes, and the communication links are its edges. The considered graph is expressed as $G = (\nu, \varepsilon, A)$ the set of nodes, ν the set of edges, and ε the adjacency matrix (in this article, A is considered time-invariant, so it is constant). a_{ij} is the weight of edge (v_i, v_j) , and if $(v_i, v_j) \in \varepsilon$, then $a_{ij} = 1$,

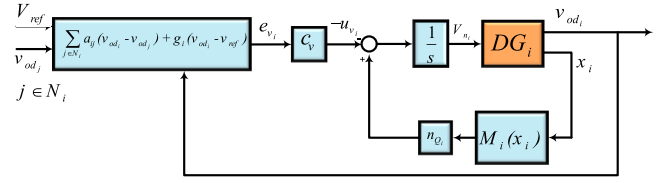


Fig. 7. Secondary voltage control of DGs in ac subgrid.

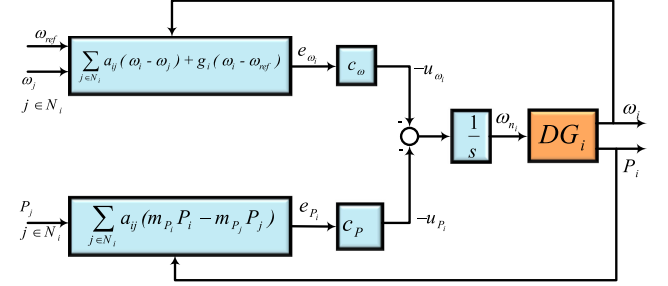


Fig. 8. Secondary frequency control of DGs in ac subgrid.

otherwise $a_{ij} = 0$. The primary strategy for i th is expressed in the synchronous reference frame (dq coordinate) as

$$v_{od_i}^* = V_{n_i} - n_{Q_i} Q_i \quad v_{oq_i}^* = 0 \quad (18)$$

where V_{n_i} is selected in such a way that $V_{o_i} \rightarrow v_{ref}$, i.e., the magnitude of voltage approaches to its reference value. By differentiating (1) and input-output feedback linearization, we have

$$\dot{v}_{od_i} = \dot{V}_{n_i} - n_{Q_i} \dot{Q}_i \equiv u_{v_i} \quad (19)$$

where u_{v_i} is the auxiliary control. Based on (19), the secondary voltage control is converted to the tracking synchronization problem for a first-order and linear MAS as

$$\begin{cases} \dot{v}_{od1} = u_{v1} \\ \dot{v}_{od2} = u_{v2} \\ \vdots \\ \dot{v}_{odN} = u_{vN} \end{cases} \quad (20)$$

These auxiliary controls are chosen based on the information of the DG and its neighbors as follows:

$$u_{v_i} = -c_v e_{v_i} \quad (21)$$

$$e_{v_i} = \sum_{j \in N_i} a_{ij} (v_{od_i} - v_{od_j}) + g_i (v_{od_i} - v_{ref}) \quad (22)$$

where g_i is mainly the weight of the edge that connects the i th DG to the reference DG [22]. Finally, the control input is given by

$$V_{n_i} = \int (u_{v_i} + n_{Q_i} \dot{Q}_i) dt \quad (23)$$

and \dot{Q}_i is described as

$$\dot{Q}_i = -\omega_c Q_i + \omega_c (v_{oq_i} i_{od_i} - v_{od_i} i_{oq_i}) \equiv M_i(x_i). \quad (24)$$

The schematics of the distributed secondary voltage and controllers of DGs in the ac subgrid are illustrated in Figs. 7 and 8, respectively. By differentiating from frequency droop characteristic, we have

$$\dot{\omega}_i = \dot{\omega}_{n_i} - m_{P_i} \dot{P}_i \equiv u_{\omega_i}. \quad (25)$$

Similarly, based on (25), we can convert the secondary voltage control problem to the tracking synchronization problem for a first-order and linear MAS and obtain

$$\begin{cases} \dot{\omega}_1 = u_{\omega_1} \\ \dot{\omega}_2 = u_{\omega_2} \\ \vdots \\ \dot{\omega}_N = u_{\omega_N} \end{cases} \quad (26)$$

$$u_{\omega_i} = -c_{\omega} e_{\omega_i} \quad (27)$$

$$e_{\omega_i} = \sum_{j \in N_i} a_{ij}(\omega_i - \omega_j) + g_i(\omega_i - \omega_{ref}) \quad (28)$$

$$\omega_{n_i} = \int (u_{\omega_i} + m_{P_i} \dot{P}_i) dt. \quad (29)$$

It is worth noting that the following equation should be satisfied by the control law:

$$m_{P_1} P_1 = \dots = m_{P_N} P_N. \quad (30)$$

The droop coefficients are chosen based on the rated active power of DGs. Therefore, we can write

$$\frac{P_1}{P_{\max_1}} = \dots = \frac{P_N}{P_{\max_N}}. \quad (31)$$

So, an additional term should be considered to meet (31). This is a regulator synchronization problem for the nonlinear and first-order MAS, which is expressed as

$$\begin{cases} m_{P_1} \dot{P}_1 = u_{P_1} \\ m_{P_2} \dot{P}_2 = u_{P_2} \\ \vdots \\ m_{P_N} \dot{P}_N = u_{P_N} \end{cases} \quad (32)$$

These auxiliary controls are chosen based on the information of the DG and its neighbors as follows:

$$u_{P_i} = -c_P e_{P_i} \quad (33)$$

$$e_{P_i} = \sum_{j \in N_i} a_{ij}(m_{P_i} P_i - m_{P_j} P_j). \quad (34)$$

Finally, the control input is expressed as (see Fig. 8)

$$\omega_{n_i} = \int (u_{\omega_i} + u_{P_i}) dt. \quad (35)$$

B. Secondary Control of DGs in DC Subgrid

In DC MGs, the decentralized droop control is considered for power-sharing among DGs (here, traditional droop control) in the first control layer of DGs in the dc subgrid so that we have (see Fig. 9) [45]

$$V_i^{\text{ref}} = V^* - r_i i_i. \quad (36)$$

The droop coefficient is selected based on the rating power of DGs, which causes voltage deviation. Therefore, increasing its value leads to more deviation. For employing the secondary voltage control of dc DGs, a signal is used and added to the traditional droop equation [37], which is given by

$$V_i^{\text{ref}} = V^* - r_i i_i + u_i. \quad (37)$$

In (37), u_i shows the added signal, which has a designing constraint. To satisfy (37), u_i should be equal in the steady-state,

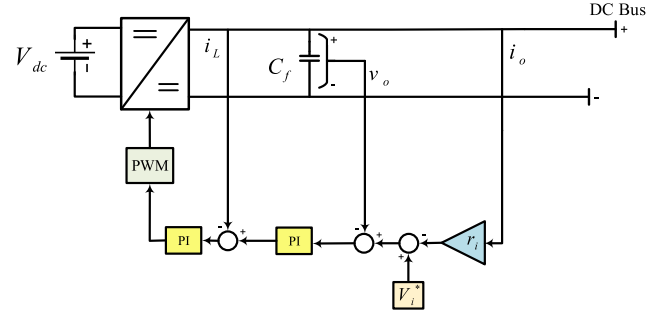


Fig. 9. Control of dc DG with primary droop control.

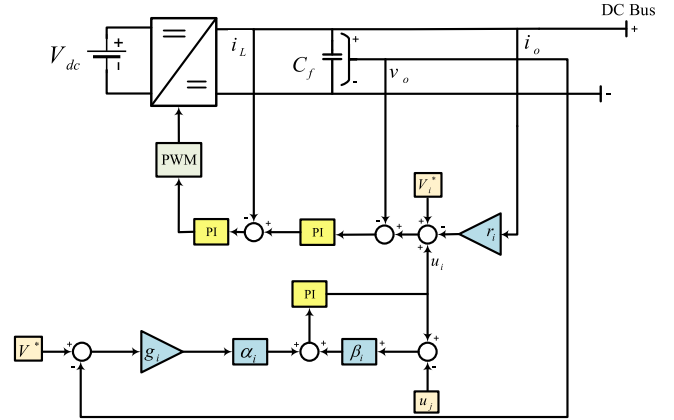


Fig. 10. Control of dc DG with secondary control.

which means

$$(u_i)^s = (u_j)^s \quad \forall i, j \quad (38)$$

where $(u_i)^s$ is the value of control input in the steady-state. To restore the parameter to its reference, the differences in the following equations should be zero:

$$e^V = V^* - V_i^{\text{ref}} \quad (39)$$

$$e^{u_t} = \sum_{j \in N_t} (u_j - u_i). \quad (40)$$

Therefore, the designed control would be

$$u_i = \left(k_{P_i} + \frac{k_{I_i}}{s} \right) e_i \quad (41)$$

where k_{P_i} and k_{I_i} are the proportional and integral PI controller for i th DG and the mixed error is defined as

$$e_i = \alpha_i e^V + \beta_i e^{u_t}. \quad (42)$$

By employing the pinning control idea, the final implemented equation would be

$$e_i = g_i \alpha_i e^V + \beta_i e^{u_t} \quad (43)$$

in which g_i is a nonzero value that shows the reference DG and has access to V^{ref} . The overall diagram of adopted distributed secondary control of DGs in the dc subgrid is illustrated in Fig. 10.

C. Control of AC/DC BIC

The converter connects the dc subgrid to a common bus. The control structure of this converter is shown in Fig. 11. As

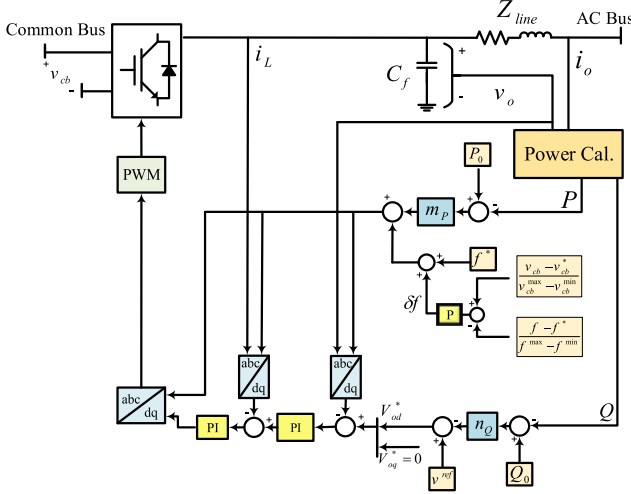


Fig. 11. Control of bidirectional ac/dc converter.

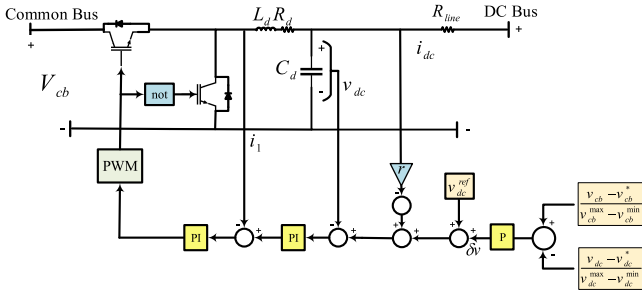


Fig. 12. Distributed control of bidirectional dc/dc converters.

observed, the output voltage is controlled by the inner loop controls to follow the reference value generated by the outer loop as [44]

$$\begin{cases} f^{\text{ref}} = (f^* + \delta f) + m_p(P - P_0) \\ v^{\text{ref}} = v^* + n_q(Q - Q_0). \end{cases} \quad (44)$$

D. Control of DC/DC BIC

The structure and control diagram of the dc/dc BIC is illustrated in Fig. 12. Because the common bus voltage is usually higher than the dc bus's voltage, this converter is considered a buck converter in which the upper side connects to a common bus. The control diagram of this converter has two control loops, too. The outer loop produces the reference value based on droop characteristic, and the inner loop controls the output of the dc voltage. This droop control law is defined as [44]

$$v_{dc}^{\text{ref}} = (v_{dc}^* + \delta v) - r \cdot i_{dc}. \quad (45)$$

It should be noted that the control scheme of ESS is the same as explained in Section II-C.

IV. SMALL-SIGNAL STABILITY STATE-SPACE MODEL

For evaluating the stability of the proposed scheme, the eigenvalue and time delay analysis were studied. To study the eigenvalue analysis, Fig. 13 is considered in which the following equations can be written for current and voltage dynamics in dq

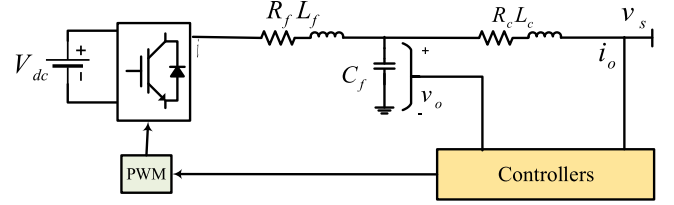


Fig. 13. Considered configuration to achieve current and voltages equations.

frame

$$\frac{di_d}{dt} = \frac{-R_f}{L_f} i_d + \omega_0 i_q + \frac{1}{L_f} (v_d - v_{od}) \quad (46)$$

$$\frac{di_q}{dt} = \frac{-R_f}{L_f} i_q - \omega_0 i_d + \frac{1}{L_f} (v_q - v_{oq}) \quad (47)$$

$$\frac{dv_{od}}{dt} = \omega_0 v_{oq} + \frac{1}{C_f} (i_d - i_{od}) \quad (48)$$

$$\frac{dv_{oq}}{dt} = -\omega_0 v_{od} + \frac{1}{C_f} (i_q - i_{oq}) \quad (49)$$

$$\frac{di_{od}}{dt} = \frac{-R_c}{L_c} i_{od} + \omega_0 i_{oq} + \frac{1}{L_c} (v_{od} - v_{sd}) \quad (50)$$

$$\frac{di_{oq}}{dt} = \frac{-R_c}{L_c} i_{oq} - \omega_0 i_{od} + \frac{1}{L_c} (v_{oq} - v_{sq}) \quad (51)$$

where v_d , v_q , i_d , and i_q are dq -axis voltages and currents; v_{od} , v_{oq} , i_{od} , and i_{oq} are dq -axis output voltages and currents; v_{sd} and v_{sq} dq -axis bus voltages; R_f , L_f and C_f the parameters of filter and R_c and L_c the resistance and inductance of line, respectively.

The instantaneous active and reactive power are also given by tow-axis theory as follows:

$$p = v_{od} i_{od} + v_{oq} i_{oq} \quad (52)$$

$$q = v_{od} i_{oq} - v_{oq} i_{od}. \quad (53)$$

By considering the linearization of (1) and (2) along with the above equations, the state-space model of a single inverter unit can be written as

$$\Delta \dot{x}_{DG} = A_{DG} \Delta x_{DG} + B_{DG} \Delta V_s \quad (54)$$

where

$$\Delta x_{DG} = [\Delta \delta \Delta P \Delta Q \Delta C_v \Delta C_c \Delta i_{dq} \Delta v_{odq} \Delta i_{odq}]^T$$

where $\Delta \delta$ is the angle difference, C_v and C_c are the states of voltage and current controllers, V_s is the supply voltage; and A_{DG} and B_{DG} are the state and input matrices, respectively. Based on this state-space model, eigenvalue analysis is provided in Section V-D.

V. SIMULATION RESULTS

For evaluating the proposed scheme's effectiveness for controlling and power management of the hybrid ac/dc MG, a hybrid ac/dc MG with multiple ac and dc DG units is simulated in MATLAB/Simulink software environment. The test hybrid ac/dc MG is shown in Fig. 14. As can be seen, the ac and dc subgrids have 3 and 4 DG units, respectively, and ac and dc subgrids are connected by ac/dc and dc/dc BICs. There is also a storage system to maintain voltage support and balance power. The storage system's output voltage is 1000 V. The

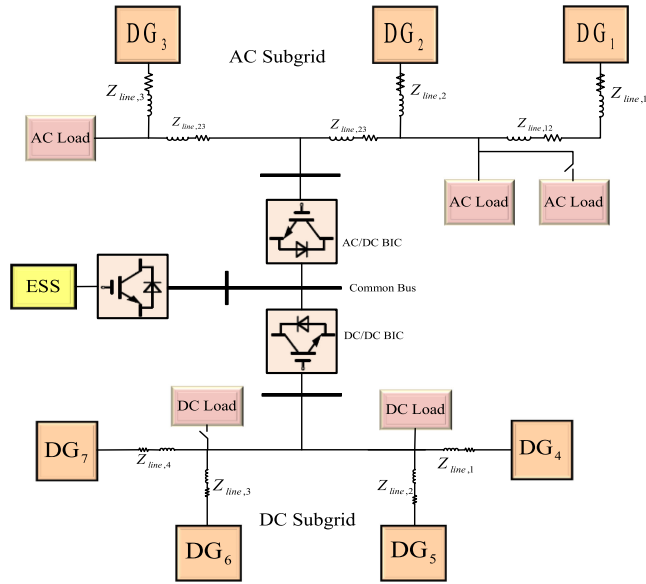


Fig. 14. Test hybrid ac/dc MG system.

TABLE I
PARAMETERS OF DGs IN AC SUBGRID

Symbol	Quantity	Value
V_{ac}^*	Nominal AC voltage	220 V
f	Nominal frequency	50 Hz
$k_{p,1-3}$	DG ₁ - DG ₃ voltage controller proportional gain	1
$k_{i,1&2}$	DG ₁ & DG ₂ voltage controller integral gain	2.5
$k_{i,3}$	DG ₃ voltage controller proportional gain	5
$k_{p,1&2}$	DG ₁ & DG ₂ current controller proportional gain	20
$k_{p,3}$	DG ₃ current controller proportional gain	10
$k_{i,1&2}$	DG ₁ & DG ₂ current controller integrsl gain	20000
$k_{i,3}$	DG ₃ current controller proportional gain	15000
$m_{p,1&2}$	DG ₁ & DG ₂ Droop coefficients	13.3×10^{-5} Hz/W
$n_{q,1&2}$		6.7×10^{-4} V/Var
$m_{p,3}$	DG ₃ Droop coefficients	5×10^{-5} Hz/W
$n_{q,3}$		4×10^{-3} V/Var
c_{ω}, c_V	Frequency & voltage control gain	400
Δf^*	Rated frequency deviation	0.5 Hz
ΔV^*	Rated voltage deviation	11 V
P_0	Rated active power for DG ₁ & DG ₂	33 kW
Q_0	Rated reactive power for DG ₁ & DG ₂	23 kVAr
P_0	Rated active power for DG ₃	25 kW
Q_0	Rated reactive power for DG ₃	15 kVAr
$k_{p,1&2}$	Proportional term of voltage controller (nonlinear method)	1
$k_{i,1&2}$	Integral term of voltage controller (nonlinear method)	500
$k_{p,1&2}$	Proportional term of current controller (nonlinear method)	100

nominal ac voltage, dc voltage, and frequency are 220, 220 V, and 50 Hz, respectively. Tables I–V show DGs' parameters in ac and dc subgrids, ac/dc and dc/dc BICs, and ESS. Impedances between DG₁ and DG₂ and between DG₂ and DG₃ are $0.23 + j 0.318 \times 10^{-3} \Omega$ and $0.175 + j 0.923 \times 10^{-3} \Omega$, respectively; and impedance between DC DGs equals to $0.268 + j 0.013 \times 10^{-3} \Omega$.

TABLE II
PARAMETERS OF DC DGs IN DC SUBGRID

Symbol	Quantity	Value
V_{dc}^*	Nominal DC voltage	220 V
k_p	Proportional term of voltage controller	4
k_i	Integral term of voltage controller	800
k_p	Proportional term of current controller	5
k_i	Integral term of voltage controller	110
$r_{1&2}$	DG ₁ & DG ₂ Droop coefficients	3 V/W
$r_{3&4}$	DG ₃ & DG ₄ Droop coefficients	2 V/W
k_p	Proportional term of secondary controller	1
k_i	Integral term of secondary controller	40
$a_{1&2}$	Nonlinear droop coefficient for DG ₁ & DG ₂	0.12 V/W
$b_{1&2}$	Nonlinear droop coefficient for DG ₁ & DG ₂	0.135 V/W
$a_{3&4}$	Nonlinear droop coefficient for DG ₃ & DG ₄	0.012 V/W
$b_{3&4}$	Nonlinear droop coefficient for DG ₃ & DG ₄	0.06 V/W

TABLE III
PARAMETERS OF AC/DC BIC

Symbol	Quantity	Value
P_0	Rated active power	33 kW
Q_0	Rated reactive power	23 kVAr
k_p	Proportional term of voltage controller	0.00001
k_i	Integral term of voltage controller	0.00002
k_p	Proportional term of current controller	0.01
m_p	Droop coefficients	11 Hz/MW
n_q		0.1 V/kVAr

TABLE IV
PARAMETERS OF DC/DC BIC

Symbol	Quantity	Value
k_p	Proportional term of voltage controller	0.6
k_i	Integral term of voltage controller	50
k_p	Proportional term of current controller	1
r	Droop coefficient	0.7 V/W
k_1	Nonlinear droop coefficient	0.02 V/W
k_2	Nonlinear droop coefficient	0.04 V/W
k_3	Nonlinear droop coefficient	0.06 V/W

TABLE V
PARAMETERS OF ESS

Symbol	Quantity	Value
V_s	Battery voltage	600 V
V_{cb}	Reference of common bus voltage	1000 V
k_p	Proportional term of voltage controller	0.0007
k_i	Integral term of voltage controller	0.07
k_p	Proportional term of current controller	8
r	Droop coefficient	$0.8 \text{ V}^2/\text{W}$

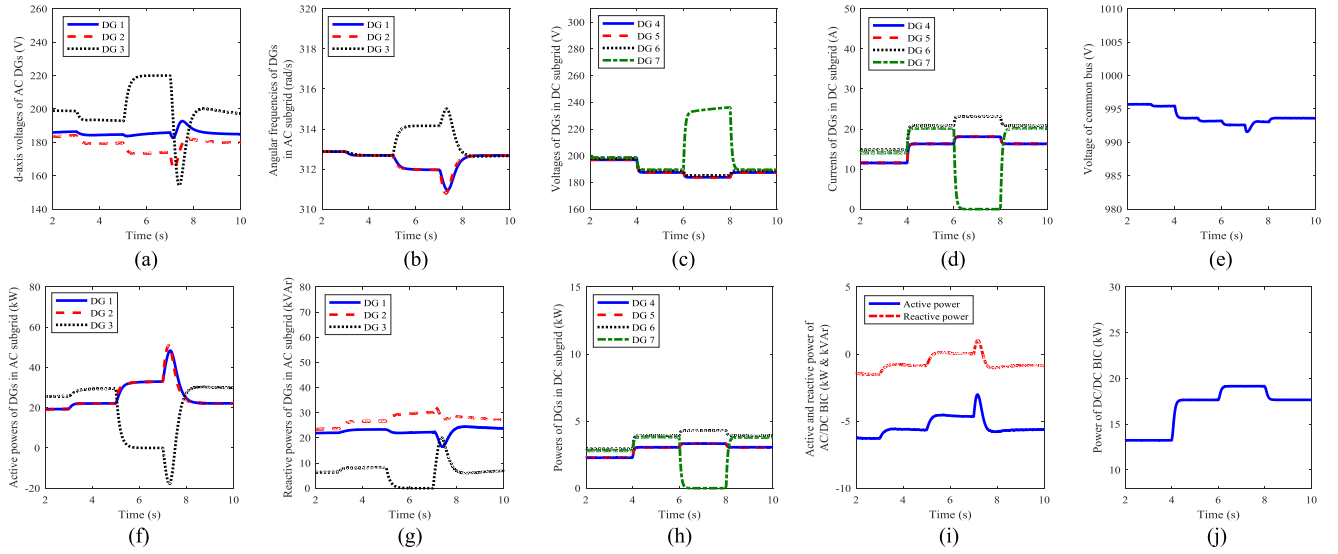


Fig. 15. Obtained results from conventional droop control [17], [43]. (a) d -axis voltages of ac DGs. (b) Angular frequencies of DGs in ac subgrid. (c) Voltages of DGs in dc subgrid. (d) Currents of DGs in dc subgrid. (e) Voltage of common bus. (f) Active powers of DGs in ac subgrid. (g) Reactive powers of DGs in ac subgrid. (h) Powers of DGs in dc subgrid. (i) Active and reactive power of ac/dc BIC. (j) Power of dc/dc BIC.

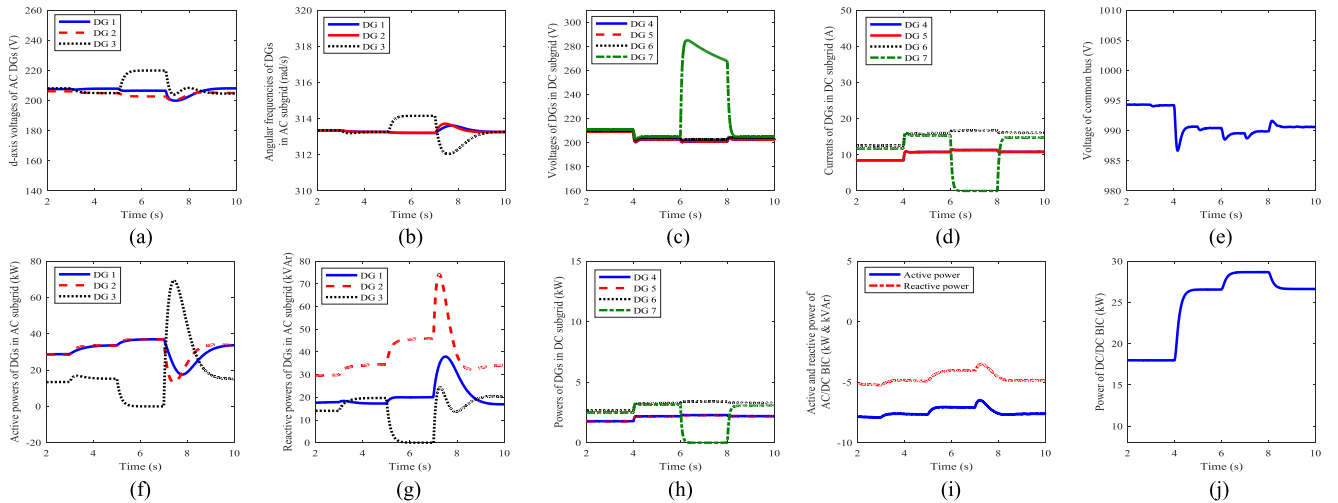


Fig. 16. Obtained results from nonlinear control. (a) d -axis voltages of ac DGs. (b) Angular frequencies of DGs in ac subgrid. (c) Voltages of DGs in dc subgrid. (d) Currents of DGs in dc subgrid. (e) Voltage of common bus. (f) Active powers of DGs in ac subgrid. (g) Reactive powers of DGs in ac subgrid. (h) Powers of DGs in dc subgrid. (i) Active and reactive power of ac/dc BIC. (j) Power of dc/dc BIC.

The AC loads in the studied MG are $30 \text{ kW} + j 20 \text{ kVAr}$ and $20 \text{ kW} + j 20 \text{ kVAr}$, and at $t = 3 \text{ s}$, a $15 \text{ kW} + j 10 \text{ kVAr}$ load is added. There are 30 and 15 kW loads in the dc subgrid, which the second load is added at $t = 4 \text{ s}$. At $t = 5 \text{ s}$, ac DG 3 is disconnected, and it is coupled at $t = 7 \text{ s}$. Finally, DC DG7 is exited at $t = 6 \text{ s}$, and then it is connected to MG at $t = 8 \text{ s}$.

A. Performance Evaluation of the Primary Controller

At first, the performance of the studied MG is investigated by activating just primary controllers. The obtained results for adopted droop control and the proposed nonlinear control schemes in the primary control level are depicted in Figs. 15 and 16. As can be observed, voltages and frequency of the studied MG are in the allowable range when the nonlinear

control is adopted (as the voltages are restored to 210 V, and the angular frequency approaches 314 rad/s). In comparison, there are considerable drops in the mentioned parameters when the MG is controlled by the conventional droop method [17], [43] (as voltages are well under 200 V, and angular frequency is just under 312.5 rad/s). As it is evident, the power-sharing with the droop control method among ac DGs, dc DGs, and ac and dc subgrids is not as precise as the proposed nonlinear method. It is worth mentioning that the common bus voltage, shown in Figs. 15–18, shows the variations of power of the whole MG. Compared with each other, the offered nonlinear method dynamics are more considerable, especially when the DGs are disconnected/connected. However, the obtained results from this strategy are closer to nominal values, and the drops in the droop method are more visible.

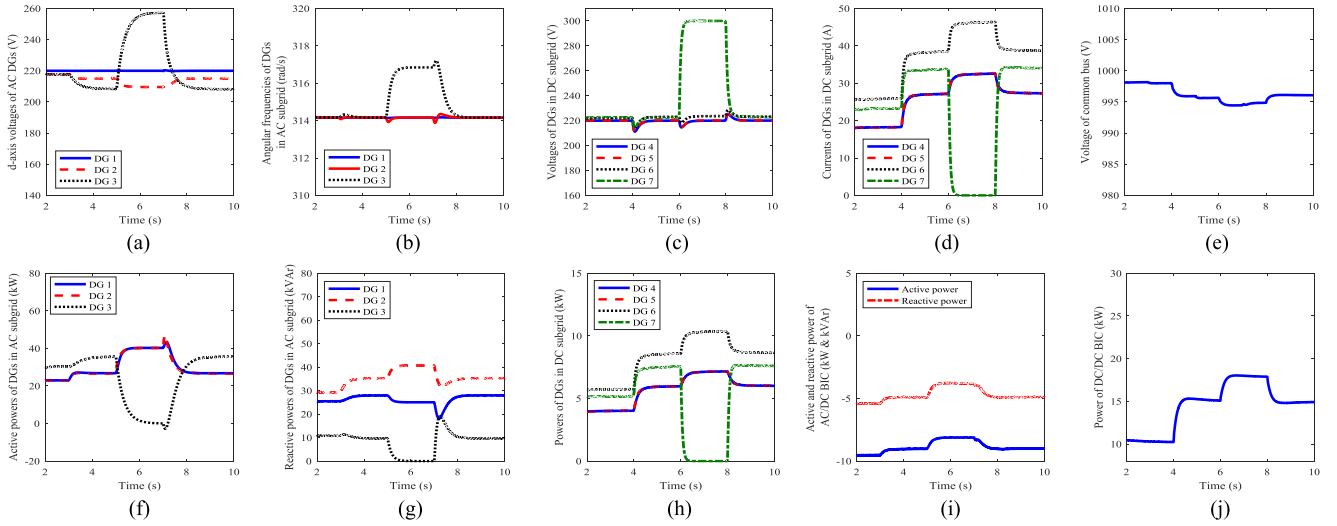


Fig. 17. Obtained results by distributed control with droop based primary control. (a) d -axis voltages of ac DGs. (b) Angular frequencies of DGs in ac subgrid. (c) Voltages of DGs in dc subgrid. (d) Currents of DGs in dc subgrid. (e) Voltage of common bus. (f) Active powers of DGs in ac subgrid. (g) Reactive powers of DGs in ac subgrid. (h) Powers of DGs in dc subgrid. (i) Active and reactive power of ac/dc BIC. (j) Power of dc/dc BIC.

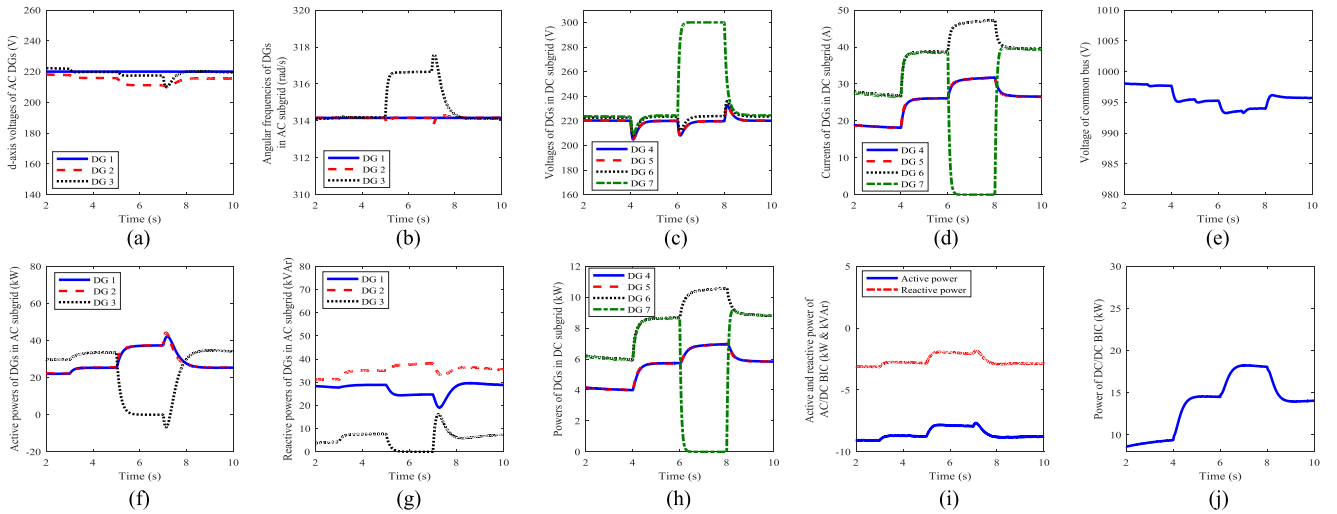


Fig. 18. Obtained results by distributed control with nonlinear based primary control. (a) d -axis voltages of ac DGs. (b) Angular frequencies of DGs in ac subgrid. (c) Voltages of DGs in dc subgrid. (d) Currents of DGs in dc subgrid. (e) Voltage of common bus. (f) Active powers of DGs in ac subgrid. (g) Reactive powers of DGs in ac subgrid. (h) Powers of DGs in dc subgrid. (i) Active and reactive power of ac/dc BIC. (j) Power of dc/dc BIC.

B. Performance Evaluation of the Primary and Secondary Controllers

For evaluating the distributed secondary control method's effectiveness, the proposed distributed control scheme is applied to the aforementioned primary control schemes in the test hybrid ac/dc MG. The adjacency matrices which illustrate the communication graph are expressed for ac and dc DGs in associated subgrids in (46) and (47), respectively.

$$\mathbf{W} = \begin{bmatrix} 0 & 0 & 1 \\ 1 & 0 & 0 \\ 0 & 0 & 1 \end{bmatrix} \quad (55)$$

$$\mathbf{B} = \begin{bmatrix} 0 & 0 & 0 & 1 \\ 1 & 0 & 0 & 0 \\ 0 & 1 & 0 & 0 \\ 0 & 0 & 1 & 0 \end{bmatrix} \quad (56)$$

The simulation results in implementing distributed secondary control are shown in Figs. 17 and 18. As can be seen, by implementing the secondary control in the studied MG, the parameters are restored appropriately to their nominal values. The voltages are restored to 220 V, and DGs' angular frequencies are fixed on 314.16, although there is an ignorable drop by increasing the loads in both subgrids. Also, the power-sharing is proper and precise, although there are some changes in loads, and some DGs are exited.

C. Eigenvalue, Time-Delay, and Robustness Analysis

In this part of the analysis, we first provide an eigenvalue analysis based on the small-signal stability state-space model presented in Section IV. Fig. 19 illustrates the considered system's eigenvalues by studying the effects of increasing the filter's capacitance, the inductance of filter, the filter's resistance,

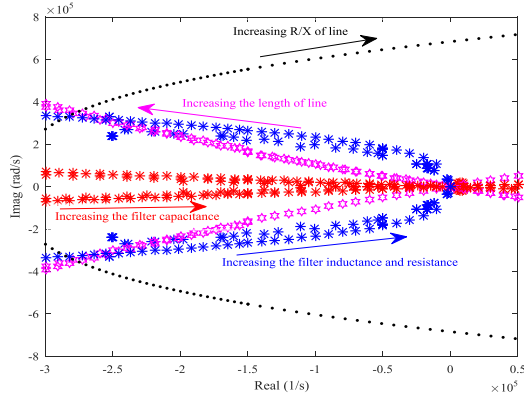


Fig. 19. Eigenvalues analysis.

increasing the R/X ratio of the line, and increasing the length of the line. As can be observed, the system is stable because all eigenvalues were on the left side of the plot while increasing the filter parameters leads used to instability. Although the R/X line increase makes the system unstable, the increasing line length causes the system to be more stable.

Next, based on the time-delay stability analysis provided in [46], a delay margin calculation is obtained to verify the proposed method. The obtained results were as $T_{\max} = 0.656$ and $\omega_{\min} = 0.987$ which lead to the system margin equals to $\tau_{\max} = 1.013$ s, while employing conventional droop control method reported in [17] and [43], τ_{\max} would be 0.837 s.

Finally, to show the system's robustness against the parametric uncertainties, robustness analysis is first converted into a polynomial problem with coefficients that structurally depend on the vector of load parameters. This polynomial is the characteristic equation of the closed-loop system denoted by $p(s, q)$, which has a multilinear uncertainty structure; namely, its coefficients depend on a multilinearly vector of uncertain parameters [47]. We also assume that set is a box containing the load parameters $q = [R \ L \ C]$. The goal is to determine the maximal uncertainty Q bounding set under which the stability of the closed-loop system or equivalently stability of the characteristic polynomial $p(s, q)$ is satisfied. Thus, the objective is to find the largest uncertainty box Q such that the family of polynomials $P = \{p(\cdot, q) : q \in Q\}$ is stable for all $q \in Q$; that is, for all $q \in Q$ all roots of $p(s, q)$ lie in the strict left half-plane. In such a case, set Q represents a *robustness margin* for the stability of the closed-loop system. A recursive calculation is required to solve the robustness margin problem. The robust stability analysis carried out in this section is explained as "the family of polynomials $P = \{p(\cdot, q) : q \in Q\}$, with uncertainty bounding set Q given by

$$Q = \begin{cases} 0.22 \text{ p.u.} \leq R \leq 10.33 \text{ p.u.} \\ 0.13 \text{ p.u.} \leq L \leq 9.09 \text{ p.u.} \\ 0.62 \text{ p.u.} \leq C \leq 26.85 \text{ p.u.} \end{cases} \quad (57)$$

is robustly stable." The proof is carried out in three steps and detailed in [47].

D. Comparison With [17], [43], and Discussion

By comprising the obtained results from the conventional droop control method, proposed nonlinear primary control strategy, and also applying the proposed distributed secondary schemes, it can be seen that when the distributed strategy is activated, the values are restored more precisely, and

the power-sharing is more proper. Although the nonlinear strategy can restore the values and propose more acceptable results compared to conventional droop control [17], [43], it has some ignorable drops and drawbacks, which are solved with a distributed control method. But, it should be noted that the proposed nonlinear method achieved acceptable results in allowable ranges without additional communication links and any secondary control layer.

For proving the superiority of the proposed method over conventional droop methods [17], [43], some indices are implemented to calculate the errors of active and reactive power and voltage and frequency distortions. These equations are described as follows:

$$e_{P_i} = \left(\frac{P_i}{\sum P_i} - \frac{P_{\text{rated},i}}{\sum P_{\text{rated},i}} \right) \times 100 \quad (58)$$

$$e_{Q_i} = \left(\frac{Q_i}{\sum Q_i} - \frac{Q_{\text{rated},i}}{\sum Q_{\text{rated},i}} \right) \times 100 \quad (59)$$

$$e_{V_i} = \left(\frac{V_{\text{rated},i} - V_i}{V_{\text{rated},i}} \right) \times 100 \quad (60)$$

$$e_{\omega_i} = \left(\frac{\omega_{\text{rated},i} - \omega_i}{\omega_{\text{rated},i}} \right) \times 100 \quad (61)$$

where e_{P_i} and e_{Q_i} are active and reactive power errors of i th DG, respectively, P_i is measured active power; Q_i is measured reactive power; $P_{\text{rated},i}$ is rated active power, and $Q_{\text{rated},i}$ is rated reactive power of i th DG, e_{V_i} and e_{ω_i} are voltage and frequency distortions of i th DG, respectively, V_i is measured voltage, ω_i is measured frequency, $V_{\text{rated},i}$ is the rated voltage, and $\omega_{\text{rated},i}$ is rated frequency of i th DG. The test microgrid system is simulated in three cases as follows, and the obtained results are given in Table VI.

- 1) Case 1: The normal operating condition.
- 2) Case 2: Load step change.
- 3) Case 3: DG plug out (outage from the grid).
- 4) Case 4: DG plugin (reconnection to the grid).

As it is evident, when there is just primary controllers, the obtained errors by implementing the nonlinear method is improved about 27%, 39%, 64%, and 44% compared to the droop method in the worst condition for active power, reactive power, voltage distortion, and frequency distortion, respectively. These improvements are 38%, 32%, 57%, and 44% for the second case study, in load step change and 19%, 32%, 58%, and 57% in plugging case study. The improvements in playing case studies are the same as improvements in the second case study. As a whole, the errors mentioned above decreased by implementing the nonlinear method instead of the conventional droop method.

When the nonlinear based primary controllers are used with secondary distributed controllers, 9%, 4%, 7%, and 0% improvements are observed in the worst conditions over droop based primary controller with secondary controllers in active power, reactive power, voltage distortions, and frequency distortions, respectively. By increasing load in case 2, the nonlinear-based method has 16%, 13%, 28%, and 0% improvements over droop based method. In case 3, the improvements are approached at 4%, 16%, 11%, and 0%. These improvements in the nonlinear based method for the fourth case study are similar to the second case study.

TABLE VI
COMPARISON OF DIFFERENT INDICES FOR VOLTAGE/FREQUENCY REGULATION AND ACTIVE/REACTIVE POWER-SHARING IN DIFFERENT CASES

Conventional droop																
Index	e_{P_i} (%)				e_{Q_i} (%)				e_{V_i} (%)				e_{ω_i} (%)			
Case	1	2	3	4	1	2	3	4	1	2	3	4	1	2	3	4
DG 1	10.3	6	13.2	6	6.8	0	9.7	0	17.5	18.2	20.5	18.2	0.45	0.5	0.7	0.5
DG 2	10.3	6	13.2	6	14	14	12.2	14	17.5	18.2	20.5	18.2	0.45	0.5	0.7	0.5
DG 3	9.8	6.1	-	6.1	30	22.8	-	22.8	9.1	11.8	-	11.8	0.45	0.5	-	0.5
DG 4	11.1	9.8	14.1	9.8	-	-	-	-	10.5	15	16.5	15	-	-	-	-
DG 5	11.1	9.8	14.1	9.8	-	-	-	-	10.5	15	16.5	15	-	-	-	-
DG 6	10.2	10.1	12.7	10.1	-	-	-	-	10	14	15.9	14	-	-	-	-
DG 7	10.2	10.1	-	10.1	-	-	-	-	10	14	-	14	-	-	-	-

Nonlinear droop																
Index	e_{P_i} (%)				e_{Q_i} (%)				e_{V_i} (%)				e_{ω_i} (%)			
Case	1	2	3	4	1	2	3	4	1	2	3	4	1	2	3	4
DG 1	8.1	4.5	10.5	4.5	5.7	4.2	8.2	4.2	5.5	5.5	6.1	5.5	0.25	0.28	0.3	0.28
DG 2	8.1	4.5	10.5	4.5	10.2	4.2	6.7	4.2	6.3	6.8	7.8	6.8	0.25	0.28	0.3	0.28
DG 3	7.6	4.8	-	4.8	18.3	15.5	-	15.5	5.4	6.8	-	6.8	0.25	0.28	-	0.28
DG 4	7.1	6.2	11.4	6.2	-	-	-	-	5.4	7.7	8.6	7.7	-	-	-	-
DG 5	7.1	6.2	11.4	6.2	-	-	-	-	5	7.7	8.6	7.7	-	-	-	-
DG 6	6.7	5.3	10.3	5.3	-	-	-	-	4.4	7.1	7.8	7.1	-	-	-	-
DG 7	6.7	5.3	-	5.3	-	-	-	-	4.1	6.8	-	6.8	-	-	-	-

Droop with distributed																
Index	e_{P_i} (%)				e_{Q_i} (%)				e_{V_i} (%)				e_{ω_i} (%)			
Case	1	2	3	4	1	2	3	4	1	2	3	4	1	2	3	4
DG 1	4.5	2	5.2	2	4	1.2	4.5	1.2	0	0	0	0	0	0	0	0
DG 2	4.5	2	5.2	2	7.1	7.1	6.1	7.1	1.1	2.2	4.5	2.2	0	0	0	0
DG 3	4	2.5	-	2.5	9.5	10	-	10	1.1	3.5	-	3.5	0	0	-	0
DG 4	3.1	1.6	5.1	1.6	-	-	-	-	0	0	0	0	-	-	-	-
DG 5	3.1	1.6	5.1	1.6	-	-	-	-	0	0	0	0	-	-	-	-
DG 6	2.8	1.4	4.8	1.4	-	-	-	-	0.9	1.4	1.6	1.4	-	-	-	-
DG 7	2.8	1.4	-	1.4	-	-	-	-	1.1	1.3	-	1.3	-	-	-	-

Nonlinear with distributed																
Index	e_{P_i} (%)				e_{Q_i} (%)				e_{V_i} (%)				e_{ω_i} (%)			
Case	1	2	3	4	1	2	3	4	1	2	3	4	1	2	3	4
DG 1	4.1	1.9	4.6	1.9	3.8	1	4.1	1	0	0	0	0	0	0	0	0
DG 2	4.1	1.9	4.6	1.9	6.8	5.7	5.1	5.7	0.9	1.8	4	1.8	0	0	0	0
DG 3	3.9	2.1	-	2.1	9.1	8.7	-	8.7	0.9	0.1	-	0.1	0	0	-	0
DG 4	2.2	1.5	5	1.5	-	-	-	-	0	0	0	0	-	-	-	-
DG 5	2.2	1.5	5	1.5	-	-	-	-	0	0	0	0	-	-	-	-
DG 6	1.7	1.1	4.6	1.1	-	-	-	-	0.9	1.4	1.7	1.4	-	-	-	-
DG 7	1.7	1.1	-	1.1	-	-	-	-	1.3	1.7	-	1.7	-	-	-	-

VI. CONCLUSION

In this article, a hybrid ac/dc MG is considered and simulated in MATLAB/Simulink software, including three DGs in the ac subgrid and four DGs in the dc subgrid in which they were connected through BICs. Two different primary control methods, i.e., conventional droop method and offered nonlinear strategy, are applied to studied MG, and their obtained results were comprised. The results showed that the nonlinear based primary control was performed better than conventional droop based primary control and had more precise power-sharing. As a whole, the reduction in active and reactive power errors was about 30%, and almost 50% improved was observed in frequency and voltage distortions. Then, the distributed based secondary control was applied to the aforementioned primary controllers to achieve more acceptable results. The secondary control method compensated the drops in voltages and frequency caused by the primary controllers and precisely restored the reference values. By implementing the secondary controllers, the active and reactive power errors decreased to about 10%, while the voltage distortion was achieved to near 15%, and frequency distortion became zero. The obtained results from simulations were comprised and showed the effectiveness and preference of the implemented nonlinear method over the conventional droop

method in restoring the values to their reference value, voltage regulation, and power-sharing. Simultaneously, by considering both cases of plug and play in the studied microgrid and changes in loads, and controllers offered acceptable and effective results.

REFERENCES

- [1] H. R. Baghaee, M. Mirsalim, G. B. Gharehpetian, and H. A. Talebi, "A decentralized power management and sliding mode control strategy for hybrid AC/DC microgrids including renewable energy resources," *IEEE Trans. Ind. Inform.*, 2017, doi: [10.1109/tii.2017.2677943](https://doi.org/10.1109/tii.2017.2677943).
- [2] Y. Xu and H. Sun, "Distributed finite-time convergence control of an islanded low-voltage AC microgrid," *IEEE Trans. Power Syst.*, vol. 33, no. 3, pp. 2339–2348, May. 2018.
- [3] M. Fakhari Moghaddam Arani and Y. A. R. I. Mohamed, "Dynamic droop control for wind turbines participating in primary frequency regulation in microgrids," *IEEE Trans. Smart Grid*, vol. 9, no. 6, pp. 5742–5751, Nov. 2018.
- [4] C. Dou, Z. Zhang, D. Yue, and M. Song, "Improved droop control based on virtual impedance and virtual power source in low-voltage microgrid," *IET Gener. Transmiss. Distrib.*, vol. 11, no. 4, pp. 1046–1054, 2017.
- [5] H. Han, Y. Liu, Y. Sun, M. Su, and J. M. Guerrero, "An improved droop control strategy for reactive power sharing in islanded microgrid," *IEEE Trans. Power Electron.*, vol. 30, no. 6, pp. 3133–3141, Jun. 2015.
- [6] R. Wang, Q. Sun, Y. Gui, and D. Ma, "Exponential-function-based droop control for islanded microgrids," *J. Modern Power Syst. Clean Energy*, vol. 7, no. 4, pp. 899–912, 2019.

- [7] A. Elrayyah, F. Cingoz, and Y. Sozer, "Construction of nonlinear droop relations to optimize islanded microgrid operation," *IEEE Trans. Ind. Appl.*, vol. 51, no. 4, pp. 3404–3413, Jul./Aug. 2015.
- [8] Q. C. Zhong, "Robust droop controller for accurate proportional load sharing among inverters operated in parallel," *IEEE Trans. Ind. Electron.*, vol. 60, no. 4, pp. 1281–1290, Apr. 2013.
- [9] H. R. Baghaee, M. Mirsalim, G. B. Gharehpetan, and H. A. Talebi, "Nonlinear load sharing and voltage compensation of microgrids based on harmonic power-flow calculations using radial basis function neural networks," *IEEE Syst. J.*, vol. 12, no. 3, pp. 2749–2759, Sep. 2018.
- [10] H. R. Baghaee, M. Mirsalim, G. B. Gharehpetan, and H. A. Talebi, "Unbalanced harmonic power sharing and voltage compensation of microgrids using radial basis function neural network-based harmonic power-flow calculations for distributed and decentralised control structures," *IET Gener. Transmiss. Distrib.*, vol. 12, no. 7, pp. 1518–1530, 2018.
- [11] Y. Gu, X. Xiang, W. Li, and X. He, "Mode-adaptive decentralized control for renewable DC microgrid with enhanced reliability and flexibility," *IEEE Trans. Power Electron.*, vol. 29, no. 9, pp. 5072–5080, Sep. 2014.
- [12] V. Nasirian, A. Davoudi, F. L. Lewis, and J. M. Guerrero, "Distributed adaptive droop control for DC distribution systems," *IEEE Trans. Energy Convers.*, vol. 29, no. 4, pp. 944–956, Dec. 2014.
- [13] S. Peyghami, H. Mokhtari, and F. Blaabjerg, "Decentralized load sharing in a low-voltage direct current microgrid with an adaptive droop approach based on a superimposed frequency," *IEEE J. Emerg. Sel. Top. Power Electron.*, vol. 5, no. 3, pp. 1205–1215, Sep. 2017.
- [14] P. Prabhakaran, Y. Goyal, and V. Agarwal, "Novel nonlinear droop control techniques to overcome the load sharing and voltage regulation issues in DC microgrid," *IEEE Trans. Power Electron.*, vol. 33, no. 5, pp. 4477–4487, May. 2018.
- [15] M. B. Delghavi and A. Yazdani, "Sliding-mode control of AC voltages and currents of dispatchable distributed energy resources in master-slave-organized inverter-based microgrids," *IEEE Trans. Smart Grid*, vol. 10, no. 1, pp. 980–991, Jan. 2019.
- [16] H. R. Baghaee, M. Mirsalim, G. B. Gharehpetan, and H. A. Talebi, "Decentralized sliding mode control of WG/PV/FC microgrids under unbalanced and nonlinear load conditions for on- and off-grid modes," *IEEE Syst. J.*, vol. 12, no. 4, pp. 3108–3119, Dec. 2018.
- [17] J. M. Guerrero, J. C. Vasquez, J. Matas, L. G. De Vicuña, and M. Castilla, "Hierarchical control of droop-controlled AC and DC microgrids - A general approach toward standardization," *IEEE Trans. Ind. Electron.*, vol. 58, no. 1, pp. 158–172, Jan. 2011.
- [18] H. R. Baghaee, M. Mirsalim, and G. B. Gharehpetan, "Power calculation using RBF neural networks to improve power sharing of hierarchical control scheme in multi-DER microgrids," *IEEE J. Emerg. Sel. Top. Power Electron.*, vol. 4, no. 4, pp. 1217–1225, Dec. 2016.
- [19] R. Heydari, T. Dragicevic, and F. Blaabjerg, "High-bandwidth secondary voltage and frequency control of VSC-based AC microgrid," *IEEE Trans. Power Electron.*, vol. 34, no. 11, pp. 11320–11331, Nov. 2019.
- [20] M. Zolfaghari, M. Abedi, and G. B. Gharehpetan, "Robust nonlinear state feedback control of bidirectional interlink power converters in grid-connected hybrid microgrids," *IEEE Syst. J.*, vol. 14, no. 1, pp. 1117–1124, Mar. 2020.
- [21] C. Wang, X. Li, L. Guo, and Y. W. Li, "A nonlinear-disturbance-observer-based DC-Bus voltage control for a hybrid AC/DC microgrid," *IEEE Trans. Power Electron.*, vol. 29, no. 11, pp. 6162–6177, Nov. 2014.
- [22] A. Bidram, A. Davoudi, F. L. Lewis, and Z. Qu, "Secondary control of microgrids based on distributed cooperative control of multi-agent systems," *IET Gener. Transmiss. Distrib.*, vol. 7, no. 8, pp. 822–831, 2013.
- [23] H. Han, X. Hou, J. Yang, J. Wu, M. Su, and J. M. Guerrero, "Review of power sharing control strategies for islanding operation of AC microgrids," *IEEE Trans. Smart Grid*, vol. 7, no. 1, pp. 200–215, Jan. 2016.
- [24] H. Zhang, S. Kim, Q. Sun, and J. Zhou, "Distributed adaptive virtual impedance control for accurate reactive power sharing based on consensus control in microgrids," *IEEE Trans. Smart Grid*, vol. 8, no. 4, pp. 1749–1761, Jul. 2017.
- [25] M. Raeispour, H. Atrianfar, H. R. Baghaee, and G. B. Gharehpetan, "Distributed LMI-based control of heterogeneous microgrids considering fixed time-delays and switching," *IET Renew. Power Gener.*, vol. 14, no. 12, pp. 2068–2078, Sep. 2020, doi: [10.1049/iet-rpg.2019.1113](https://doi.org/10.1049/iet-rpg.2019.1113).
- [26] M. Raeispour, H. Atrianfar, H. R. Baghaee, and G. B. Gharehpetan, "Resilient H_∞ consensus-based control of autonomous AC microgrids with uncertain time-delayed communications," *IEEE Trans. Smart Grid*, vol. 11, no. 5, pp. 3871–3884, Sep. 2020.
- [27] A. Afshari, M. Karrari, H. R. Baghaee, G. B. Gharehpetan, and S. Karrari, "Cooperative fault-tolerant control of microgrids under switching communication topology," *IEEE Trans. Smart Grid*, vol. 11, no. 3, pp. 1866–1879, May. 2020.
- [28] A. Afshari, M. Karrari, H. R. Baghaee, and G. B. Gharehpetan, "Resilient cooperative control of AC microgrids considering relative state-dependent noises and communication time-delays," *IET Renew. Power Gener.*, vol. 14, no. 8, pp. 1321–1331, 2020.
- [29] A. Afshari, M. Karrari, H. R. Baghaee, and G. B. Gharehpetan, "Resilient synchronization of voltage/frequency in AC microgrids under deception attacks," *IEEE Syst. J.*, 2020, doi: [10.1109/JSYST.2020.2992309](https://doi.org/10.1109/JSYST.2020.2992309).
- [30] J. Lai, H. Zhou, X. Lu, X. Yu, and W. Hu, "Droop-based distributed cooperative control for microgrids with time-varying delays," *IEEE Trans. Smart Grid*, vol. 7, no. 4, pp. 1775–1789, Jul. 2016.
- [31] N. M. Dehkordi, H. R. Baghaee, N. Sadati, and J. M. Guerrero, "Distributed noise-resilient secondary voltage and frequency control for islanded microgrids," *IEEE Trans. Smart Grid*, vol. 10, no. 4, pp. 3780–3790, Jul. 2019.
- [32] A. Afshari, M. N. Karrari, H. R. Baghaee, and G. B. Gharehpetan, "Distributed fault-tolerant voltage/frequency synchronization in autonomous AC microgrids," *IEEE Trans. Power Syst.*, vol. 35, no. 5, pp. 3774–3789, Sep. 2020, doi: [10.1109/tpwrs.2020.2975115](https://doi.org/10.1109/tpwrs.2020.2975115).
- [33] A. Pilloni, A. Pisano, and E. Usai, "Robust finite-time frequency and voltage restoration of inverter-based microgrids via sliding-mode cooperative control," *IEEE Trans. Ind. Electron.*, vol. 65, no. 1, pp. 907–917, Jan. 2018.
- [34] H. Cai and G. Hu, "Distributed nonlinear hierarchical control of AC microgrid via unreliable communication," *IEEE Trans. Smart Grid*, vol. 9, no. 4, pp. 2429–2441, Jul. 2018.
- [35] A. M. Shotorbani, S. Ghassem-Zadeh, B. Mohammadi-Ivatloo, and S. H. Hosseini, "A distributed secondary scheme with terminal sliding mode controller for energy storages in an islanded microgrid," *Int. J. Elect. Power Energy Syst.*, vol. 83, no. 1, pp. 352–364, 2017.
- [36] W. W. A. G. Da Silva, T. R. Oliveira, and P. F. Donoso-Garcia, "Hybrid distributed and decentralized secondary control strategy to attain accurate power sharing and improved voltage restoration in DC microgrids," *IEEE Trans. Power Electron.*, vol. 35, no. 6, pp. 6458–6469, Jun. 2020.
- [37] F. Guo, Q. Xu, C. Wen, L. Wang, and P. Wang, "Distributed secondary control for power allocation and voltage restoration in islanded DC microgrids," *IEEE Trans. Sustain. Energy*, vol. 9, no. 4, pp. 1857–1869, Oct. 2018.
- [38] T. Morstyn, M. Momayyezani, B. Hredzak, and V. G. Agelidis, "Distributed control for state-of-charge balancing between the modules of a reconfigurable battery energy storage system," *IEEE Trans. Power Electron.*, vol. 31, no. 11, pp. 7986–7995, Nov. 2016.
- [39] B. Wang et al., "Consensus-based control of hybrid energy storage system with a cascaded multiport converter in DC microgrids," *IEEE Trans. Sustain. Energy*, vol. 11, no. 4, pp. 2356–2366, Oct. 2020.
- [40] P. Lin et al., "A distributed power management strategy for multi-paralleled bidirectional interlinking converters in hybrid AC/DC microgrids," *IEEE Trans. Smart Grid*, vol. 10, no. 5, pp. 5696–5711, Sep. 2019.
- [41] H. J. Yoo, T. T. Nguyen, and H. M. Kim, "Consensus-based distributed coordination control of hybrid AC/DC microgrids," *IEEE Trans. Sustain. Energy*, vol. 11, no. 2, pp. 629–639, Apr. 2020.
- [42] T. Logenthiran, R. T. Naayagi, W. L. Woo, V. T. Phan, and K. Abidi, "Intelligent control system for microgrids using multiagent system," *IEEE J. Emerg. Sel. Top. Power Electron.*, vol. 3, no. 4, pp. 1036–1045, Dec. 2015.
- [43] A. Khorsandi, M. Ashourloo, H. Mokhtari, and R. Iravani, "Automatic droop control for a low voltage DC microgrid," *IET Gener. Transmiss. Distrib.*, vol. 10, no. 1, pp. 41–47, 2016.
- [44] Y. Xia, W. Wei, M. Yu, X. Wang, and Y. Peng, "Power management for a hybrid AC/DC microgrid with multiple subgrids," *IEEE Trans. Power Electron.*, vol. 33, no. 4, pp. 3520–3533, Apr. 2018.
- [45] P. H. Huang, P. C. Liu, W. Xiao, and M. S. El Moursi, "A novel droop-based average voltage sharing control strategy for DC microgrids," *IEEE Trans. Smart Grid*, vol. 6, no. 3, pp. 1096–1106, May. 2015.
- [46] H. R. Baghaee, M. Mirsalim, G. B. Gharehpetan, and H. A. Talebi, "A generalized descriptor-system robust H_∞ control of autonomous microgrids to improve small and large signal stability considering communication delays and load nonlinearities," *Int. J. Elect. Power Energy Syst.*, vol. 92, pp. 63–82, 2017.
- [47] H. Karimi, A. Yazdani, and R. Iravani, "Robust control of an autonomous four-wire electronically-coupled distributed generation unit," *IEEE Trans. Power Del.*, vol. 26, no. 1, pp. 455–466, Jan. 2011.